POLITECNICO DI TORINO
Repository ISTITUZIONALE

Mapping Transition Metal-Nitrogen-Carbon Catalysts Performance on the Critical Descriptors Diagram

(Article begins on next page)

23 April 2024

Mapping Transition Metal-Nitrogen-Carbon Catalysts Performance on the Critical Descriptors Diagram

Stefania Specchia[1*], Plamen Atanassov[2], José H. Zagal[3]

[1] Department of Applied Science & Technology, Politecnico di Torino, Corso Duca degli Abruzzi 24, 10129 Torino, Italy; stefania.specchia@polito.it

[2] Department of Chemical & Biomolecular Engineering and National Fuel Cell Research Center, University of California Irvine, CA 92697, USA; plamen.atanassov@uci.edu

[3] Laboratorio de Electrocatálisis y Electrónica Molecular, Departamento de Química de los Materials, Universidad de Santiago de Chile, Ada. Bernardo Ohiggins 3363, Santiago 9170022, Chile; jose.zagal@usach.cl

Graphical abstract
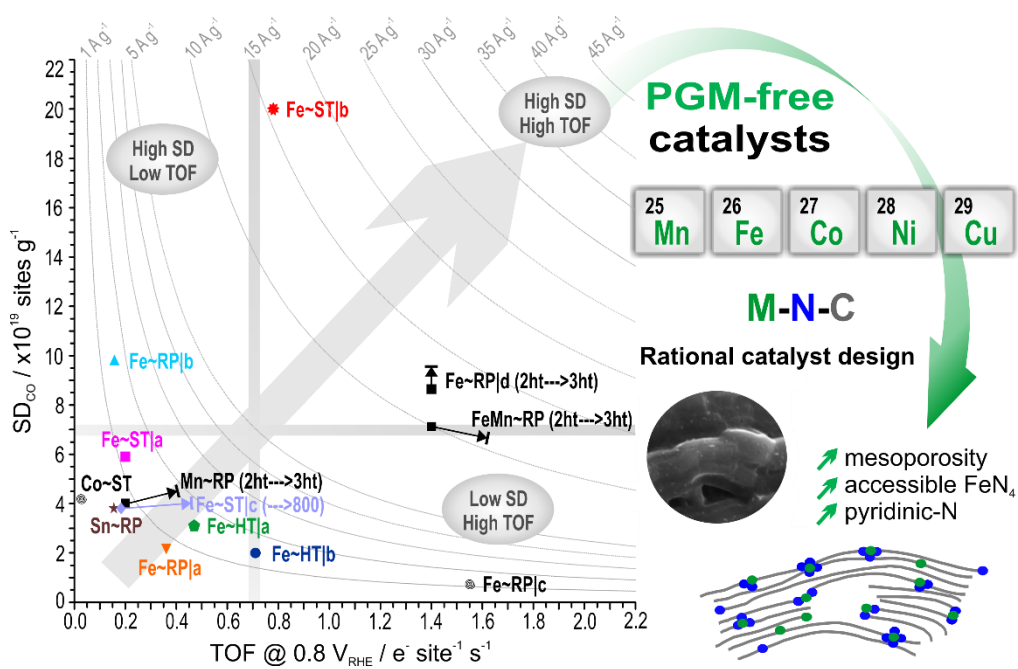
Highlights

- Site density vs. ORR turn-over frequency for PGM-free catalysts from the literature.
- Rational catalyst design: + mesoporosity, + accessible FeN_4 centers, + pyridinic-N.
- Crucial role of the precursors and synthesis method in catalysts formation.

Abstract

PGM-free electrocatalysts, and in particular transition metal-nitrogen-carbon (M-N-C) catalysts are becoming interesting candidates as cheap alternatives to Pt-based catalysts for the oxygen reduction reaction (ORR) in polymer electrolyte fuel cells (PEFC). Unified activity-stability correlations are needed in order to provide practical guidelines for a rational catalyst design. A discussion of different characterization techniques for studying possible activity descriptors is presented, with a specific focus on active-site density (*SD*) and turn-over frequency (*TOF*). These descriptors will be associated to the morphology of the various M-N-C electrocatalysts investigated in the recent literature. The underlined correlation for this class of PGM-free electrocatalysts offers important insights required for the development of the next-generation of catalytic materials with enhanced stability, that can solve the main activity and durability barriers needed for the replacement of Pt-based counterparts.

Introduction

Although polymer electrolyte fuel cells (PEFCs) are recognized worldwide as pollution-free and high-performance devices, their mass commercialization is still a long way off [1–4],

mostly because they are still an expensive technology. Almost 50% of the cost, in fact, is attributable to Pt-based catalysts [5]. Platinum group metals (PGM) on earth are scarce and expensive. A high amount of Pt is necessary to favor the oxygen reduction reaction (ORR), which is a well-known sluggish electrode reaction [6]. To overcome such a bottleneck, transition metal (Fe,Co)/nitrogen-doped carbon structures (M-N-C materials) have been widely investigated in the last decades due to their great electrocatalytic activity for ORR [7–15]. M-C-C materials have also extraordinary tolerance to alcohols, a beneficial property for direct alcohols fuel cells (DAFCs) [16,17]. Notwithstanding all the research efforts, these materials still suffer from low activity compared to PGM catalysts, and stability is still an issue [18–23]. As stated more than ten years ago by Gasteiger and Markovic [1], only via rational catalyst design routes we can push the overall intrinsic activity of M-N-C catalysts close to that of Pt-based materials.

According to the targets established by the U.S. Department of Energy (DOE), the specific activity of PGM-free catalysts implemented in a H_2/O_2 PEFC operating at 1 bar at 0.9 $V_{iR-free}$ is expected to be 44 mA cm^{-2} [5], to be competitive compared to PGM electrocatalysts. This activity target is equivalent to the PGM activity target calculated from the product of mass activity, 440 mA mg$_{Pt}^{-1}$, and the target Pt cathode loading of 0.100 mg$_{Pt}$ cm^{-2} [5]. The two best activities recorded so far with Fe-N-C catalysts reach only 75% and 66% of this target (33 mA cm^{-2} with a catalyst prepared from zeolitic imidazolate framework (ZIF) via chemical vapor deposition (CVD) [24] and 29 mA cm^{-2} with a catalyst prepared from ZIF via reactive polymerization [25], the latter reached within the ElectroCat Consortium [26]).

Active Site Density and Turn-Over Frequency: Two Critical Descriptors

To better understand the activity of PGM-free catalysts, scientists disclosed several descriptors to identify the nature of the active sites towards ORR, which is still under debate. In fact, not only Fe-N$_4$ active sites, but also Fe-moieties and Fe-free moieties can contribute to the ORR [13]. Among them, the most typical descriptors debated in the literature are structural ones, usually determined by N$_2$ sorption measurements, ^{57}Fe Mössbauer spectroscopy, X-ray photoelectron spectroscopy (XPS), X-ray absorption near-edge spectroscopy (XANES), X-ray photoelectron and mass spectroscopy (EXAFS), neutron

activation analysis, and with the help of density functional theory (DFT) calculations [19,27–30], and reactivity ones, such as redox potential of the FeN_x or CoN_x active centers, adsorption energy of intermediate products and work function [31–37]).

Nowadays, two reactivity descriptors, the active metal gravimetric site density, SD [$site\ g_{cat}^{-1}$], and the catalytic turn-over frequency, TOF [$electron\ site^{-1}\ s^{-1}$], are becoming predominant since their combination discloses the catalysts' intrinsic kinetic activity at a selected potential, $J_{kin,mass}$ [$A\ g^{-1}$], as clearly explained by Zagal et al. [38]. Thus, the evaluation of TOF and SD is recognized as one of the most accurate comparisons among different catalysts [39].

The SD can be measured by *ex situ* cryo CO chemisorption or *in situ* adsorption of NO_2^- [38]. Interestingly, by observing SD values of some catalysts reported in **Table 1**, measured on the same catalysts by CO chemisorption and NO_2^- adsorption, the resulting SD_{NO2} is always smaller compared to the SD_{CO}. The reason lies in the ability of the CO molecules to easily access the porosity of the catalysts, especially the microporosity, thus reaching more active sites. Primbs at al. [40] correlated the gaseous CO uptake on the basis of SD_{CO} calculation with the specific surface, pore structure, and bulk weight Fe content. Whereas the correlation was weaker with SD_{NO2}. In fact, against a set of four catalysts with different physico-chemical characteristics (**Table 1**: Fe~ST|a [40], Fe~RP|a [40,41]; Fe~HT|a [40,42]; Fe~HT|b [40,43]), the larger difference between the two values of SD belongs to the catalyst with the largest specific volume of micropores, and the smallest specific volume of mesopores (Fe~ST|a). This is a clear sign that active sites present in micropores are accessible only by probe CO molecules, while they are hidden from NO_2^-.

Recently, Kumar et al. [44] demonstrated the NO_2^- adsorption method can provide SD values, which include not only contributions from the FeN_4 active sites, but also from other species, such as Fe_2O_3. The authors performed a deep study on fresh/aged $Fe_{0.5}/NC$ and Fe_2O_3/NC catalysts, calculating that the Fe_2O_3/NC catalyst displayed a slightly higher SD but lower TOF compared to the more active fresh $Fe_{0.5}/NC$, being rich of only FeN_x sites (**Tables 1** and **2** [44]). This is a demonstration that SD_{NO2} measurements are sensitive to the presence of FeO species. The authors also evaluated the SD/TOF values before/after a series of

accelerated stress tests (AST) on the $Fe_{0.5}$/NC catalyst. AST in presence of oxygen under potential cycling (AST-OPC: 0.6-1.0 V vs RHE) caused a large decrease of the mass activity of the aged $Fe_{0.5}$/NC, mainly due to carbon corrosion. This was accompanied by an unexpected +40% of the *SD* value and −50% of the *TOF* value compared to the fresh $Fe_{0.5}$/NC (**Table 1**, [44]). A combination of electrochemical experiments and chemical/morphological characterizations on the aged catalyst pointed out that more Fe atoms were exposed on the surface because of the presence of reactive oxygen species (ROS) which enhanced carbon corrosion. These Fe atoms were no longer solely in the form of FeN_x sites, but with a prevalence of FeO, due to the re-precipitation of Fe cations reacting with ROS to form Fe oxides [44]. Moreover, carbon corrosion was preferentially on structurally disordered domains, leaving the more graphitic domains almost unaffected [45]. This work also pointed out the effects of ageing on the change of chemical-morphological structure of Fe-N-C catalysts. The shift of Fe species from FeN_x to FeO combined with the preferential corrosion of disordered carbon was labelled as ROS-induced carbon corrosion [44]. Furthermore, other research on deactivation of Fe-N-C catalysts [33] demonstrated that the presence of H_2O_2 leaves FeN_x sites untouched but enhances the reversible oxidation of the carbon surface. Consequently, the ORR activity is reduced and the *TOF* decreased via weakened O_2 binding. In fact, catalysts containing only Fe particles encapsulated in a graphitic shell do not suffer deactivation (no iron exposed on the surface), but are intrinsically less active. Therefore, the chemical-morphological characterization of the catalysts is of utmost importance to better understand the origin of the activity, and to determine the correct values of *SD* and *TOF* for a proper comparison of different catalytic materials, at fresh and aged states. Moreover, the mismatching *SD* and *TOF* values, determined by the NO_2^- adsorption method, compared to mass activity values unravel the sensitivity of the analysis to both FeN_x and FeO species, by highlighting the complexity and plurality of the degradation mechanisms of Fe-N-C catalysts.

The Case of Heat-Treated Transition Metal-Nitrogen-Carbon Catalysts

Most of the PGM-free catalysts are prepared by mixing reactants and pyrolyzing them under specific conditions of temperature, atmosphere, and time. The pyrolysis leads to a series of chemical and morphological transformations with the formation of active sites, that nature of which is still under debate [13]. However, these materials exhibit much

higher activity and stability compared to intact (not pyrolyzed) PGM-free catalysts [38,46]. A relevant difference between Fe-N-C materials and intact macrocyclic FeN_4 complexes is the difference in the inner N_4 coordination around the metal center. For Fe-N-C materials, there is evidence of pyridinic ligation fused with graphite layers whereas for the majority of intact MN_4 metal complexes they feature pyrrolic ligation. These differences have been characterized in detail by ^{57}Fe Mössbauer spectra, XPS and atomic-resolution TEM of both intact and pyrolyzed materials. For example, Marshall-Roth et al. [47] have recently reported the preparation of Fe complexes based on phenanthroline hexaazamacrocycle, $(phen_2N_2)Fe$, that feature a pyridinic N_4 coordination environment around Fe, similar to that of Fe-N-C materials with high *TOF* (1.8 s^{-1}) for ORR in acid.

The pyrolysis and the nature of precursors used for the synthesis of Fe-N-C materials lead to a plurality of Fe-based active sites: $Fe-N_4$, $Fe-N_3$, $Fe-N_2$, $Fe-N_{2+2}$, $Fe-N_{4+1}$, $N-Fe-N_{2+2}$, $Fe-N_xC_{4-x}$, Fe-nanoparticles (α-Fe and γ-Fe), Fe-nitrides and Fe-carbides, usually termed as Fe-containing moieties active sites [13]. All of these sites can be available for ORR, depending on their location: in-plane and out-of-the-plane, on the edge of carbon crystallites, encapsulated in the carbon matrix, etc. [13,44]. Each of them is contributing to the overall activity of the catalyst, either by acting on the *TOF* (the higher the *TOF*, the more active the site is) or the *SD* (the higher the *SD*, the more the active sites are).

Thus, the critical rational design question is: Is it more advantageous to synthesize catalysts with a higher *TOF*, or to aim synthesis efforts at achieving a higher *SD*?

Let us observe **Figure 1**, showing the SD_{CO} versus *TOF* map of Fe-based catalysts derived from different precursors. The values are taken from different publications, at equal conditions on rotating(-ring) disk electrode (RDE or RRDE) at 0.8 V_{RHE} and *SD* measured by *ex-situ* CO chemisorption. **Table 1** lists the punctual values depicted in the figure. **Table 2** lists a brief summary on the synthesis processes used to prepare these catalysts. The materials have been subdivided into three main "families" of catalysts depending on the nature of the precursors used, and the type of synthesis:

- Catalysts derived from ZIF precursors via soft-templating (M~ST: Fe~ST|a [40], Fe~ST|b [24]); Fe~ST|c [48], Co~ST [49,50];
- Catalysts derived from polyaniline (PANI) or diaminonaphtalene precursors via reactive polymerization (M~RP: Fe~RP|a [40,41]; Fe~RP|b [49], Fe~RP|c [51], Fe~RP|d [52]49, Mn~RP[52], FeMn~RP[52], Sn~RP [49];
- Catalysts derived from organic precursors and SiO₂ via hard-templating (M~HT: Fe~HT|a [40,42]; Fe~HT|b [40,43], the latter a commercial catalyst from Pajarito Powder [43]).
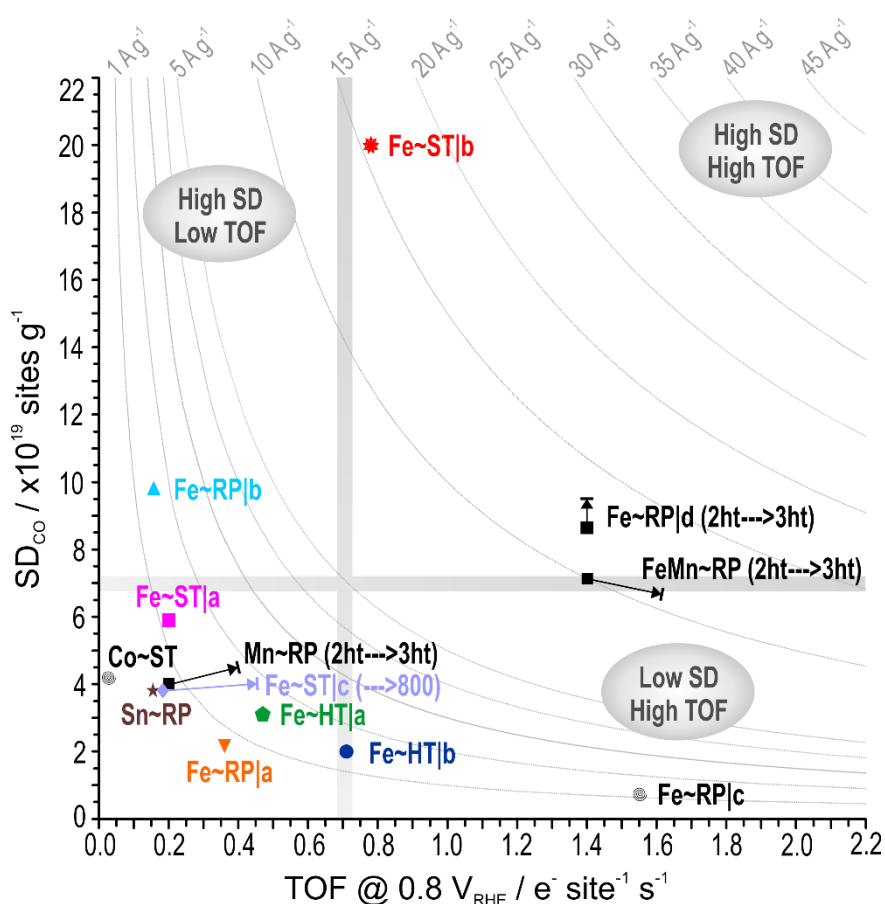
Figure 1. Map of gravimetric active-site density vs ORR turn-over frequency for a series of PGM-free catalysts from the literature (measurements performed in RDE or RRDE). Reactivity map resulting from *SD* measured by CO chemisorption. Hyperbolic iso-activity curves in A g^{-1} at 0.8 V$_{RHE}$ are also reported. Catalysts abbreviations: M~ST derived from soft-templating; M~RP derived from reactive polymerization (M~RP|2ht→3ht → reactive

polymerization followed by 2 or 3 heat treatments); M~HT derived from hard-templating (for synthesis methods, see **Table 2**).
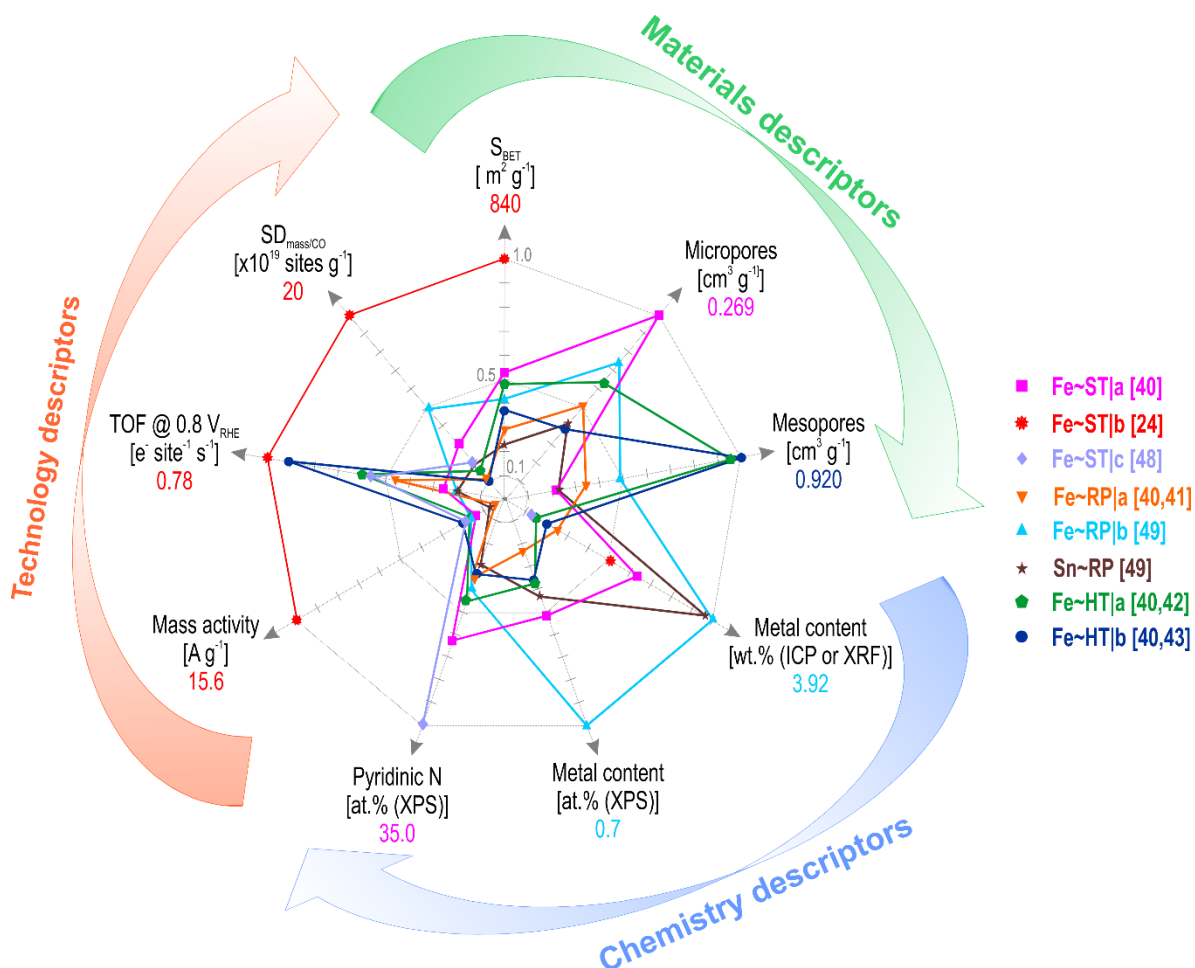
Figure 2. Radar plot of the colored catalysts in **Figure 1** for a relative comparison of the main physico-chemical data (exact values listed in **Table 1**). The three main descriptor categories are highlighted. Catalysts abbreviations: M~ST derived from soft-templating; M~RP derived from reactive polymerization; M~HT derived from hard-templating Data taken from the literature.

By subdividing the map into four quadrants, from low to high values of *SD* and *TOF*, we observe different behaviors. The three catalysts derived from the soft templating of ZIF, Fe~ST|a, Fe~ST|c, and Co~ST, lie in the lower quadrant, with low *TOF* and *SD* values. The mass activity is extremely low, as well. Apparently, the amount of active sites is similar, but the activity of the Co-based catalyst is negligible. Interestingly, when Fe~ST|c is further heat-treated at 800 °C under CO atmosphere, both the mass activity and *TOF* results increased by about 60%, while the *SD* increased only slightly (**Table 1**). The different rate of variation of *TOF* and *SD* point towards the formation of more intrinsic active sites rather than the formation of new active sites, such as a different thermally-induced FeN_x site distribution [48]. Looking at the radar plot, **Figure 2**, the Fe~ST|a catalyst has the highest value of micropores and pyridinic-N, which are notoriously two characteristics known to favor the formation of active sites [27,53].

Interestingly, the Fe~ST|b catalyst, which is derived from a nanosized ZIF-8, lies in the upper quadrant, with a *TOF* value comparable to others in the literature, and an extremely high *SD* value, equivalent to the 47% Pt/C catalysts [39]. High values of *SD* are extremely beneficial in MEA testing, especially at high current densities where transport limitations dominate [12,19,54,55]. In fact, the Fe~ST|b catalyst tested on H_2/O_2 PEFC, reached an activity of 33 mA cm^{-2} at 0.90 $V_{iR-free}$ [24]. This exceptional result, which pushes this catalyst to the top-center of the map, can be ascribed to its morphological characteristics. In fact, this catalyst has a high mesoporosity (**Table 1**), tuned via the CVD technique. According to the authors, flowing $FeCl_3$ on a bed of N-C material (**Table 2**) led to the formation of high number of Fe-N_4 active sites, mostly located on the outer surface of the starting carbonaceous matrix, thus easily accessible to oxygen. The physico-chemical characterization highlighted the formation of a catalyst with an extremely high specific surface area and abundance of micro/mesopores, and abundance of Fe-N_4 moieties, compared to other Fe-based active sites [24]. It is known that larger pores favor the creation of a triple-phase boundary in PEFC electrodes, which are less affected by flooding during MEA operation [17,42]. The CVD synthesis route translated into the creation of a highly active catalyst, with a boosted activity toward the ORR. Interestingly, at the optimized temperature of 750 °C, the vapor of $FeCl_3$ reacts with Zn-N_4 from the ZIF starting precursor, leading to the formation of Fe-N_4 and release of $ZnCl_2$. Such a reaction occurs only on the surface of the carbon matrix, where $ZnCl_2$ can easily evaporate,

leading to the formation of Fe-N_4 active sites on the catalyst surface. The active sites located on the surface are more accessible, enabling the enhanced ORR activity [12]. This effect, together with the extraordinarily high specific surface area, gives rise to an extremely active catalyst. Similar effects of increased FeN_4 structures in the near edges of the carbon matrix have also been obtained by adding specific hydrogen donor/accepter functionalities near the active sites [12,56], yielding superior electroactivity performances and *TOF* values (1.1 e$^-$ site^{-1} s^{-1}, reached in the Electrocat Consortium [26]). A higher CVD temperature was not effective due to the decrease of the N content [57,58], with consequent reduction of the Fe-N_4 active sites. For this catalyst, Jiao et al. [24] estimated the different types of Fe moieties present in the catalyst via XPS and ^{57}Fe Mössbauer spectroscopy, and *in situ* XAS. Specifically, they calculated two utilization factors: U_{Fe}, defined as the ratio of the Fe atoms present as Fe-N_4 moieties with respect to the total Fe atoms in the catalyst, and U_{FeN4}, defined as the ratio of the gas-phase accessible Fe-N_4 moieties with respect to all Fe-N_4 moieties present in the catalyst. Based on these definitions, the authors re-defined the *SD* based on the bulk Fe amount in the catalyst. They obtained U_{Fe} = 0.9 and U_{FeN4} = 1, demonstrating that Fe~ST|b has a high density of Fe-N_4 sites, all of which are available for ORR. These values for U_{Fe} and U_{FeN4} are much higher compared to those of similar Fe-N-C catalysts, at analogous total Fe amounts [40,59]. Notably, compared to Fe~ST|b, Fe~ST|a has much lower U_{FeN4}, but higher Fe content (**Table 1** and radar plot **Figure 2**), suggesting that in this catalyst most of the Fe-N_4 sites are inaccessible to oxygen. This is also corroborated by the very different, and lower values of SD_{NO2} compared to SD_{CO} [40]. In fact, CO as probe molecule penetrates better into pores, reaching a higher number of active sites, and giving rise to higher values of SD_{CO}.

Remarkably, Wan et al. [59] well-correlated the relationship among *SD*, *TOF*, porosity, and Fe content by synthesizing a series of very active catalysts (the best of which, TPI@Z8(SiO$_2$)-650-C reached a power density of 1.18 W cm^{-2} in a 2.5 bar H$_2$/O$_2$ PEFC). The catalysts where synthesized by combining two different synthesis methods, soft templating by ZIF and hard templating by SiO$_2$, for a better tuning of the morphology, obtaining an extremely high specific surface area with enlarged mesopores (**Table 1**). By increasing the amount of Fe, these authors observed a huge increase of SD_{NO2}, while the *TOF* values remained almost unchanged. On the other hand, U_{Fe} decreased with the increase of

Fe. They established a structure-property correlation for which the large external surface area and mesoporosity play crucial roles in maximizing *SD*, which is the predominant factor in determining a high current density at the PEFC level. In fact, the exposure of Fe-N$_4$ active sites to oxygen enhances mass transport properties in the catalytic layer of the MEA [46].

In **Figure 1**, catalysts Fe~RP|a, Fe~HT|a, Fe~HT|b, and Sn~RP are in the lower bottom/left quadrant, with low *TOF* and medium/low *SD* values. Interestingly, Fe~HT|a and Fe~HT|b exhibit the highest mass activity in this quadrant (**Table 1**). Both these catalysts are prepared by hard templating, that is by mixing silica powder with Fe nitrate and carbendazim, pyrolyzing at high temperature, and etching the silica [42]. The hard templating procedure produces a self-supported catalyst with an open-frame morphology [60], characterized by high specific surface area, many mesopores, and relatively low Fe content but high pyridinic-N (**Table 1** and radar plot in **Fig. 2**). Such a morphology displays a better activity compared to those of ZIF-derived catalysts mentioned above, but much lower compared to the catalysts prepared by CVD. The radar plot is very similar for these catalysts. Notably, Fe~HT|a has an intermediate value of *U$_{FeN4}$*, of 0.43, with an enhancement of the intrinsic activity.

In the low *SD* / low *TOF* quadrant, we also found the Sn~RP catalyst, prepared by using Sn instead of Fe, with reactive polymerization of aniline (**Table 2**). This catalyst displays values in line with the other catalysts of the same quadrant, with relatively low values of all the physico-chemical characteristics, as evident from the radar plot (**Fig. 2**).

For a further enhancement of the mass activity, we have to move toward the top-left or bottom-right quadrants of the *SD* vs *TOF* map. In these quadrants, we find the catalysts Fe~RP|b and Fe~RP|c, both produced by reactive polymerization. No data are available for Fe~RP|c, but for Fe~RP|b the comparative radar plot highlights high values of Fe content, micro- and meso-porosity (**Table 1** and **Fig. 2**).

Sahraie et al. [52] prepared a series of mono- and bimetallic catalysts by reactive polymerization, mixing Fe and Mn: Fe~RP|d, Mn~RP, and bimetallic FeMn~RP. To better quantify the density and utilization of the active sites, they studied the effect of two or three heat treatments followed by acid leaching (**Table 2**). Interestingly, looking at the mono Fe-

N-C catalyst, the three steps of the heat treatment helped to slightly improve the *SD* values, at equal *TOF*. The heat treatment did not affect the nature of the active sites, which exchange the same number of electrons, but increased their availability to oxygen (**Fig. 1**: the black arrow indicated an increased in the *SD* of the Fe~RP|d from 2ht to 3ht). When Mn was added, with only two heat treatments, the *SD* was slightly reduced at equal *TOF*. However, a third heat treatment slightly changed the nature of the active sites, resulting in a higher *TOF*, but slightly lower *SD*, following the behavior of Mn~RP. More interestingly, the utilization factor U_{Fe}, increased with the number of heat treatments for both Fe~RP|d and FeMn~RP (**Table 1**). Notably, the heat treatment not only favored the formation of more active sites, but also increased the accessibility of the active sites to ORR. These results were supported by a slight increase of the surface-near elemental atomic Fe content when Mn was added, as measured by XPS (**Table 1**). Therefore, the mass activity was pushed in a favorable way toward the top/right quadrant of the *SD* vs *TOF* map.

Observing the two figures and the nature of active sites highlighted in the third column of **Table 2**, it is clear that the *TOF* depends on the physico-chemical properties of the support. It is difficult to determine possible correlations to elucidate which FeN_x active site has the greatest enhancement on the *TOF* value. For example, in the comparative work of Primbs et al. [40], the highest activity belongs to Fe~HT|b, Fe~HT|a, and Fe~ST|a, respectively, which contain a plurality of active sites as FeN_x and Fe nanoparticles (Fe(III)N_4 and Fe(II)N_4, α-Fe and γ-Fe). Interestingly, Fe~HT|b has the highest Fe utilization factor U_{Fe}, linked to the accessibility of the FeN_x sites. But the most stable catalyst under AST cycling is the less active Fe~RP|a, which contains a higher amount of only atomically dispersed Fe(III)N_4 and Fe(II)N_4 active sites, and the lowest U_{Fe}. In this work [40], Fe~ST|a was synthesized intentionally to contain a much higher content of Fe as compared to the "twin" catalysts synthesized by Zitolo et al. [58] with the same procedure but lower amounts of atomic Fe. Here, Fe$_{0.5}$-NC (containing only atomically dispersed FeN_x species) has almost the same activity of Fe$_{1.0}$-NC (containing atomically dispersed FeN_x, Fe nanoparticles and Fe carbide), but much higher stability under AST cycling. In agreement with the results of Primbs et al. [40]. Moreover, Zitolo et al. [58] demonstrated that the activity of Fe$_{0.5}$-NC can be enhanced

by pyrolysis with NH_3. In fact, NH_3 increases the basicity of the carbon support, favoring the formation of FeN_4C_{12} moieties [61,62].

Very recently, the porphyrin-like high-spin MN_4C_{12} moiety (M = Fe [63,64] and Co [64]) has been identified as a highly active site towards ORR, leading to high values of *TOF*. Interestingly, the CoN_4C_{12} moiety is slightly less active but more stable than the FeN_4C_{12} moiety. On one hand, Li et al. [63] identified two active sites in their fresh $Fe_{0.5}$-NC catalyst: a high-spin surface FeN_4C_{12} and a low-spin FeN_4C_{10} not accessible to oxygen (no Fe metal or other Fe species). Upon prolonged potential cycling in oxygen, they found a decreased amount of the FeN_4C_{12} moiety, mostly by demetallation and localized carbon surface oxidation (in agreement with [33,45]), while the amount FeN_4C_{10} remained constant. Indicating that the surface FeN_x active sites are non-durable, moving irreversibly from Fe(III) to Fe(II) as ferric oxide (in agreement with Zitolo et al. [58]). Conversely, the FeN_x active sites buried into the carbon matrix remained stable, and active towards ORR. Similarly, Xie et al. [64] compared the activity of Fe-N-C and Co-N-C catalysts, synthesized to have the same atomic percentage of metal and the same morphology (dominant microporous structure, only atomically dispersed MN_4C_{12} moieties, no nanoparticles and carbides present). At the fresh state, the two catalysts displayed similar activity, but Co-N-C was 4-folds more durable under potential cycling in oxygen. Oxygen promoted Fe demetallation from FeN_4C_{12} moieties, since Fe catalyzes the Fenton reactions to a larger extent compared to Co. A detailed cross-linking of Mössbauer and XANES analyses coupled with DFT calculations confirmed that Co has a higher resistance to metal leaching compared to Fe. Predicted free energy barriers for demetallation showed higher values for Co compared to Fe. Thus, the stability of Co is correlated with the Co-N bond length, which is shorter compared to the Fe-N bong length. The shorter bond length of M-N, the higher the free energy [65].

Apparently, those catalysts containing a plurality of FeN_x sites and Fe particles buried in the carbon, thus not available for ORR at the fresh state, display lower activity at the beginning of life, but higher stability [33,45]. The exposure to ageing protocols leads to dramatic changes in the morphological structure of the catalyst, which in turn provokes changes more accentuated on *TOF* rather than *SD*.

Concluding on the observation of the map and radar plot, we can answer our question: high TOF values are more desirable, than high SD values. Accessibility of Fe-N$_4$ active sites plays a key-role on the catalyst activity. However, it is critical that less accessible active sites must simultaneously be present to enhance catalyst durability. Only a tailored and rational synthesis method can allow for an increase both of active and stable sites. The morphology of the catalyst, especially in terms of macropores, pyridinic-N, and porphyrin-like FeN$_4$C$_{12}$ sites, plays a crucial role in increasing the number of active sites placed not only on the outer surface of the carbon matrix, but also buried into it. On the contrary, too much bulk Fe is not effective. With the progresses made in the recent years, the Pt vs Fe gap on TOF values has been reduced from a factor x100 to x20 and further improvements are possible.

Table 1. Main physico-chemical data of the catalysts reported in **Fig. 2.** Mass activity measured by RDE or RRDE.
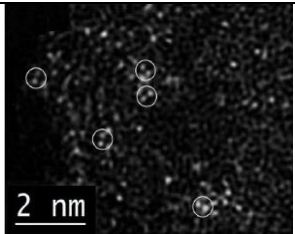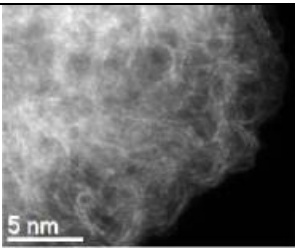
Catalyst [ref.]	S_{BET} [m² g⁻¹]	Micro-/mesopore volumes [cm³ g⁻¹]	Metal content [wt.% (ICP) / at.% (XPS)]	Pyridinic-N [at.% (XPS)]	Measured mass activity @ 0.8 V_{RHE} [A g⁻¹]	TOF @ 0.8 V_{RHE} [e⁻ site⁻¹ s⁻¹] TOF_{CO} / TOF_{NO2}	SD_{mass} [x10¹⁹ site g⁻¹] SD_{CO} / SD_{NO2}	U_{Fe} factor [-]
Fe~ST|a [40]	840	0.269 / 0.203	2.5 / 0.36	21.6	2.2	0.200 / 0.14	5.8 / 1.5	0.35
Fe~ST|b [24]	1593	- / -	2.0 / -	-	15.6	0.780 / -	20 / -	0.90
Fe~ST|c [48]	-	-	- / < 0.5	36.0	1.11	0.18 / -	3.84 / -	-
Fe~ST|c(800) [48]	-	-	- / < 0.5	35.0	2.86	0.45 / -	3.99 / -	-
Co~ST [49,50]	-	- / -	1.00 / 0.40	23.8	0.2	0.029 / -	4.2 / -	-
Fe~RP|a [40,41]	463	0.137 / 0.317	1.0 / 0.16	12.8	0.6	0.360 / 0.44	2.2 / 1.7	0.20
Fe~RP|b [49]	665	0.200 / 0.450	3.92 / 0.70	14.0	2.4	0.156 / -	9.8 / -	-
Sn~RP [49]	364	0.110 / 0.210	3.78 / 0.30	9.7	0.9	0.155 / -	3.8 / -	-
Fe~RP|c [51]	531	- / -	1.5 / -	-	-	1.550 / -	0.72 / -	-
Fe~RP|d_2ht [52]	-	- / -	12 / -	-	-	1.4 / -	8.9 / -	0.082
Fe~RP|d_3ht [52]	-	- / -	6.00 / 0.33	-	21	1.4 / -	9.1 / -	0.162
Mn~RP|2ht [52]	-	- / -	9 / 0.5	-	-	0.2 / -	4.0 / -	-
Mn~RP|3ht [52]	-	- / -	5 / 0.5	-	3.0	0.4 / -	4.3 / -	-
FeMn~RP|2ht [52]	-	- / -	5 (Fe) 3 (Mn) / -	-	-	1.4 / -	7.1 / -	0.124
FeMn~RP|3ht [52]	-	- / -	3 (Fe) 1 (Mn) / 0.58 (Fe)	-	17.6	1.6 / -	6.7 / -	0.231
Fe~HT|a [40,42]	763	0.181 / 0.880	0.6 / 0.26	15.4	2.5	0.470 / 0.46	3.1 / 0.6	0.43
Fe~HT|b [40,43]	593	0.103 / 0.920	0.8 / 0.25	11.6	3.1	0.710 / 0.8	2.0 / 0.2	0.78
Fe₂O₃/NC [44]	-	-				- / 1.2	- / 0.59	-
Fe₀.₅/NC fresh [44]	-	-	- / 1.3		6.50	- / 7.1	- / 0.45	-
Fe₀.₅/NC aged [44] -	-	-	- / 0.26* (see. **Table 2**)		2.94	- / 4.4	- / 0.62	-
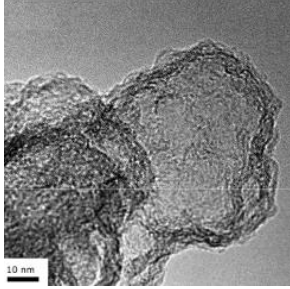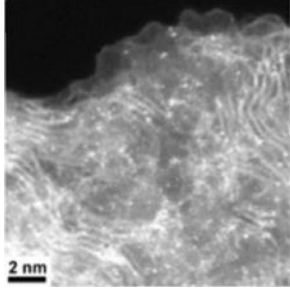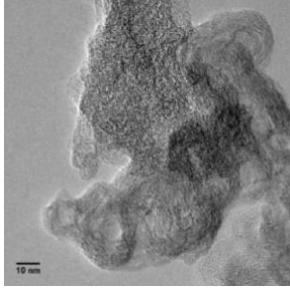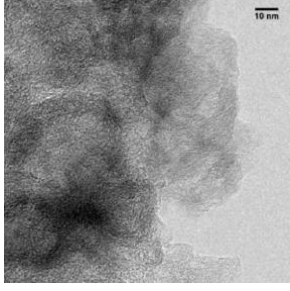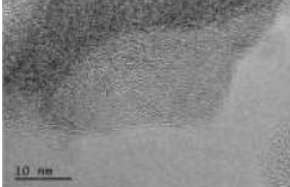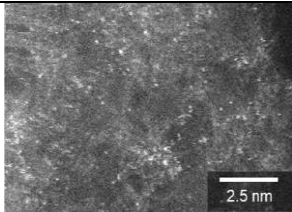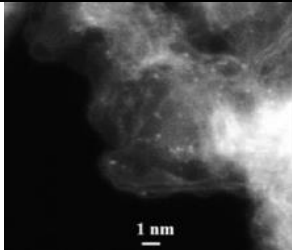
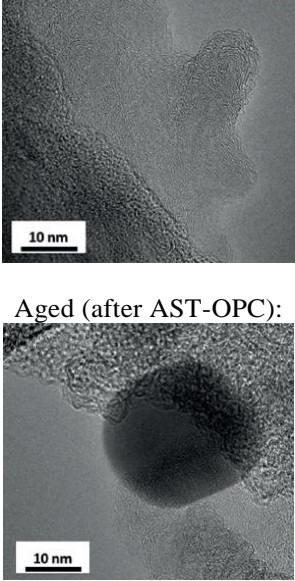| TPI@Z8(SiO$_2$)-650-C family [59]	1648	40% / 60%	from 0.283 to 2.7 at.%			- / from 1.57 to 1.63	- / from 22.0 to 56.8 μ g^{-1}	from 0.44 to 0.19

Table 2. Main physico-chemical characteristics of the catalysts reported in **Figure 1**. Data taken from the literature (n.a.: not available).

Catalyst [ref.]	Schematic synthesis	Nature of the active sites and absolute wt% or relative % of each Fe species [from ^{57}Fe Mössbauer]	Morphology [from HAADF-STEM/TEM]
Fe~ST|a [40]	Dry ball milling of ZIF-8 nanocrystals, Fe(II) acetate, and 1,10-phenanthroline. Ball-milling. Pyrolysis 1 h @ 1050 °C in Ar.	D1 high-spin Fe(III)N$_4$: 0.88 wt% D2 low-spin Fe(II)N$_4$: 0.62 wt% Magnetic α-Fe: 0.55 wt% Non-magnetic γ-Fe: 0.36 wt% Fe$_3$C: 0.09 wt%	
Fe~ST|b [24]	Preparation of nanosized Zn(II) zeolitic imidazolate framework (ZIF-8). Mixing nanosized ZIF-8 and phenanthroline in ethanol and drying. Homogenization via low energy ball milling. Pyrolysis under Ar @ 1050 °C. The resulting N-C powder and FeCl$_3$ as precursor placed in two separate ceramic boats, and pyrolyses 3 h @ 750 °C in Ar followed by cooling for the CVD of Fe on N-C.	D1 O$_2$-Fe(III)-N$_4$: 89% (air-accessible) relative area D3 high spin Fe(II)Cl$_2$: 11%	
Fe~ST|c Fe~ST|c_ 800 [48]	Fe(II) acetate, 1,10-phenanthroline, and ZIF-8, a Zn(II) zeolitic imidazolate framework mixed in a planetary ball miller with 4 cycles of 30 min each at 400 rpm. Flash pyrolysis under Ar flow at 1050°C for 1 h, followed by a fast cooling in cold Ar flow. For the Fe~ST|c_800 sample: sequence of cleaning, CO uptake, and desorption cycles at the annealing temperature of 800°C.	Atomically dispersed FeN$_4$ moieties as D1 low-spin Fe(II)N$_4$ and D2 median-spin Fe(II)N$_4$. For the Fe~ST|c_800 sample: increased content of graphitic N.	n.a.

Co~ST [49,50]	Zn(II) zeolitic imidazolate framework (ZIF-8), phenanthroline and Co(II) acetate ball-mixed with 4 cycles of 30 min each. The resulting powder pyrolyzed 1 h @ 1050 °C in Ar. Final activation in a flow of NH_3 maintained for 2 h at 750 °C	From EXAFS measurement and DFT analysis: atomically dispersed cobalt ions and electronic state of three porphyrinic moieties: CoN_4C_{12}, $CoN_3C_{10,porp}$ and CoN_2C_5.	
Fe~RP|a [40,41]	Mixing of di-amino naphthalene $C_{10}H_{10}H_2$, APS $(NH_4)_2S_2O_8$ and $FeCl_2$ in ethanol to form oligomers in a shape of self-assembled nanospheres. Drying. Heat treatment 2 h @ 1000 °C in N_2.	D1 high-spin $Fe(III)N_4$: 0.35 wt% D2 low-spin $Fe(II)N_4$: 0.65 wt%	
Fe~RP|b [49]	$FeCl_3$ dissolved in aniline and HCl. In situ polymerization with APS $(NH_4)_2S_2O_8$. Addition of activated Ketjenblack. Resulting refluxed C/$FeCl_3$/PANI: ball-milled. Three steps of pyrolysis (1st: 1 h @ 900 °C in N_2; 2nd and 3rd: 3 h @ 900 °C in N_2) with intermediate two acid leaching (1 M H_2SO_4), washing and drying.	Atomically dispersed D1 and D2 doublets assigned to FeN_4 moieties of different oxidation and spin states.	
Sn~RP [49]	Solution of aniline and HCl. In situ polymerization with APS $(NH_4)_2S_2O_8$. Addition of activated Ketjenblack. Resulting refluxed C/PANI mixed with anhydrous $SnCl_2$ and ball-milled. Three steps of pyrolysis (1st and 2nd: 1 h @ 900 °C in N_2; 2nd and 3rd: 3 h @ 900 °C in N_2) with intermediate two acid leaching / washing / drying steps (4 M HCl).	^{119}Sn Mössbauer (relative %): Sn(IV)-a: 30.6% Sn(II)-b: 47.7% Mixed ionic/covalent: 21.7%	
Fe~RP|c [51]	Mixing of di-amino naphthalene $C_{10}H_{10}H_2$, APS $(NH_4)_2S_2O_8$ and $FeCl_2$ in ethanol to form self-assembled oligomeric nanospheres.	n.a.	

	Solvent evaporation. 1st heat treatment 2 h @ 950 °C in N₂. Acid leaching in 0.5 M H₂SO₄. Drying. 2nd heat treatment 2 h @ 900 °C in N₂.		
Fe~RP|d 3ht [52]	Monometallic catalysts: FeCl₃ (or MnCl₂) dissolved in aniline and HCl. In situ polymerization with APS (NH₄)₂S₂O₈. Addition of Ketjenblack. Resulting C/FeCl₃/PANI heat treated with 2 or 3 steps of pyrolysis (1st: 1 h @ 900 °C in N₂; 2nd and 3rd: 3 h @ 900 °C in N₂) followed by 1 or 2 steps of intermediate acid leaching (2 h @ 900 °C in 2 M H₂SO₄, washing and drying). For the bimetallic catalyst: FeCl₃/MnCl₂ molar ratio = 1/1.	D1 low spin $Fe(II)N_4$: 1.33 wt% D2 intermediate spin Fe(II)Pc: 2.66 wt% D3 $(NFe(III)N_4)$-O_2: 0.44 wt% D4 high spin XY-FeN_4 (XY weak O and/or N ligands): 0.56 wt% Oxidized magnetic Fe particles: 1.02 wt%	n.a.
Mn~RP 3ht [52]		n.a.	n.a.
FeMn~RP 3ht [52]		D1 low spin $Fe(II)N_4$: 1.17 wt% D2 intermediate spin Fe(II)Pc: 1.11 wt% D3 $(NFe(III)N_4)$-O_2: 0.43 wt% Oxidized magnetic Fe particles: 0.29 wt%	n.a.
Fe~HT|a [40,42]	Dispersion of silica in water, addition of carbendazim and ultrasonication, addition of iron nitrate $Fe(NO_3)_3$ and further ultrasonication. Drying. Grounding. 1st pyrolysis 1.5 h @ in N₂. Adic leaching in 25 wt.% HF. Washing & drying. 2nd pyrolysis 30 min h @ 950 °C in NH₃.	D1 high-spin $Fe(III)N_4$: 0.28 wt% D2 low-spin $Fe(II)N_4$: 0.39 wt% Non-magnetic γ-Fe: 0.13 wt%	2.5 nm
Fe~HT|b [40,43]	Hard templating with fumed silica, commercially named as PMF-011904 (Pajarito Powder Inc.).	D1 high-spin $Fe(III)N_4$: 0.05 wt% D2 low-spin $Fe(II)N_4$: 0.19 wt% Magnetic α-Fe: 0.10 wt% Non-magnetic γ-Fe: 0.27 wt%	1 nm
Fe₀.₅/NC [44]	Fe(II) acetate, 1,10-phenanthroline and ZIF-8 (0.5 wt % Fe in the precursor), mixed in a planetary ball-miller at 400 rpm for 2 h. Ramp pyrolysis in Ar up to 1050°C at 5°C min⁻¹, stay	Fresh Fe₀.₅/NC: Atomically dispersed D1 and D2 doublets, confirmed by EXAFS with peaks of Fe-N and Fe-C backscatterings in FeN_xC_y moieties. Aged Fe₀.₅/NC (after AST-OPC), by TEM, EDX and Raman	Fresh catalyst:

| | at 1050°C for 1 h, fast quenching under Ar. | analyses: FeN_xC_y moieties and many particles of 10-50 nm attributed to FeO and $Fe_{0.90}$ (Wüstite). Local Fe content (**Table 1**): 0.26 at.% (EDX local analysis, cannot be considered as the average Fe content) | |
| | | | Aged (after AST-OPC): |

Conclusions and Outlook

We attempted to discuss in a concise form the characteristics of M-N-C electrocatalysts and bring the comparative study of their performance in RDE/RRDE to two main descriptors: (i) turn-over frequency (*TOF*) for ORR at a high potential of 0.8 V vs. RHE and (ii) site density (*SD*) expressed per unit mass of catalyst. This initial and simplified discussion leaves untouched the accessibility of the active sites as the next critical parameter. For most M-N-C catalysts only N_2 gas-accessible surface area (S_{BET}) is reported, while the electrochemically accessible surface area (*ECSA*) for PGM-free catalysts, including the M-N-C class, is not universally measured, and is rarely discussed. Water retention isotherms are not studied or published for these materials, and their hydrophobicity/hydrophilicity relationship to morphology is widely unexplored. All these materials and surface parameters will need to be combined into at least one morphology-dependent parameter (such as active site accessibility), expressed through roughness factor, Thiele modulus or effectiveness factor for the catalyst. This discussion naturally brings the structural parameters of the catalysts' particle to the level of aggregate, agglomerate and ultimately to catalyst layer (CL) design associated with the membrane electrode assembly (MEA) integration. The ultimate performance improvement and "moving the performance point" in **Fig. 1** simultaneously to

higher *TOF* and *SD* values (the desired outcome of the catalysts design) will depend on the successful implementation of new synthesis routes for designing catalysts with more accessible and stable active with high *SD* and *TOF*. The high *TOF* catalysts have specific synthesis barriers to overcome, especially considering the mass transport phenomena in the CL of MEAs, not discussed here. The observations provided here are leaving us with an optimistic picture that activity issues are clearly addressable within available technology and might already have been *de-facto* addressed in the laboratories of many groups pursuing M-N-C design.

What remains a great challenge, however, is the stability of catalysts during long-term operation. Along with specific atomistic factors of M-N-C active site deactivation (de-metalation), poisoning (usually reversible) and carbonaceous backbone material corrosion under fuel cell operating conditions (all the time above the thermodynamic stability potential of carbon oxidation), we would also bring attention to the possible role of morphological transformations during fuel cells' operation. Without forgetting the emerging need for such changes to be captured in *durability descriptors*, that should be integrated with the M-C-N *catalytic activity descriptors* discussed in this overview.

Conflict of Interest Statement

The authors declare that they have no known competing financial interests or personal relationships that could have appeared to influence the work reported in this paper.

Credit Author Statement

The authors contribute equally to the work by discussing and writing the manuscript, drawing the figures, along with approving its final version.

Acknowledgements

References

[1]   H.A. Gasteiger, N.M. Marković, Just a Dream—or Future Reality?, Science (80.). 324 (2009) 48–49. doi:10.1126/science.1172083.

[2]   A. Brouzgou, S.Q. Song, P. Tsiakaras, Low and non-platinum electrocatalysts for PEMFCs: Current status, challenges and prospects, Appl. Catal. B Environ. 127 (2012) 371–388. doi:10.1016/j.apcatb.2012.08.031.

[3]   B.G. Pollet, S.S. Kocha, I. Staffell, Current status of automotive fuel cells for sustainable transport, Curr. Opin. Electrochem. 16 (2019) 90–95. doi:10.1016/j.coelec.2019.04.021.

[4]   A. Coralli, B. Sarruf, P.E.V. de Miranda, L. Osmieri, S. Specchia, N.Q. Minh, Fuel cells, in: P.E.V. de Miranda (Ed.), Sci. Eng. Hydrog. Energy Technol., Elsevier Inc., 2019: pp. 39–122. doi:10.1016/B978-0-12-814251-6.00002-2.

[5]   S.T. Thompson, A.R. Wilson, P. Zelenay, D.J. Myers, K.L. More, K.C. Neyerlin, D. Papageorgopoulos, ElectroCat: DOE's approach to PGM-free catalyst and electrode R&D, Solid State Ionics. 319 (2018) 68–76. doi:10.1016/j.ssi.2018.01.030.

**[6] N. Ramaswamy, S. Mukerjee, Influence of inner- and outer-sphere electron transfer mechanisms during electrocatalysis of oxygen reduction in alkaline media, J. Phys. Chem. C. 115 (2011) 18015–18026. doi:10.1021/jp204680p.

An outstanding paper explaining complex electrochemical reactions such as ORR involving multi-electron transfer depending on the nature of the electrode surface. The main differences between ORR in acid and alkaline media are clearly elucidated.

[7]   T.S. Olson, B. Blizanac, B. Piela, J.R. Davey, P. Zelenay, P. Atanassov, Electrochemical evaluation of porous non-platinum oxygen reduction catalysts for polymer electrolyte fuel cells, Fuel Cells. 9 (2009) 547–553. doi:10.1002/fuce.200800089.

[8]   M. Shao, Q. Chang, J.-P. Dodelet, R. Chenitz, Recent Advances in Electrocatalysts for Oxygen Reduction Reaction, Chem. Rev. 116 (2016) 3594–3657. doi:10.1021/acs.chemrev.5b00462.

[9]   A.H.A. Monteverde Videla, L. Osmieri, S. Specchia, Non-noble metal (NNM) catalysts for fuel cells: Tuning the activity by a rational step-by-step single variable evolution, in: J.H. Zagal, B. Fethi (Eds.), Electrochem. N_4 Macrocycl. Met. Complexes Vol. 1 Energy, Second Ed., 2nd ed., Springer Nature, Switzerland, 2016: pp. 69–102. doi:10.1007/978-3-319-31172-2_3.

[10]   H.M. Barkholtz, D.J. Liu, Advancements in rationally designed PGM-free fuel cell catalysts derived from metal-organic frameworks, Mater. Horizons. 4 (2017) 20–37. doi:10.1039/c6mh00344c.

[11]   L. Osmieri, L. Pezzolato, S. Specchia, Recent trends on the application of PGM-free catalysts at the cathode of anion exchange membrane fuel cells, Curr. Opin. Electrochem. 9 (2018) 240–256. doi:10.1016/j.coelec.2018.05.011.

[12]   U. Martinez, S. Komini Babu, E.F. Holby, H.T. Chung, X. Yin, P. Zelenay, Progress in the Development of Fe-Based PGM-Free Electrocatalysts for the Oxygen Reduction Reaction, Adv. Mater. 31 (2019) 1806545. doi:10.1002/adma.201806545.

**[13]T. Asset, P. Atanassov, Iron-Nitrogen-Carbon Catalysts for Proton Exchange Membrane Fuel Cells, Joule. 4 (2020) 33–44. doi:10.1016/j.joule.2019.12.002.

An outstanding review paper providing a view on how chemical composition and morphology impact on the reactivity and stability of highly active PGM-free catalysts.

[14]   L. Osmieri, J. Park, D.A. Cullen, P. Zelenay, D.J. Myers, K.C. Neyerlin, Status and challenges for the application of platinum group metal-free catalysts in proton-

exchange membrane fuel cells, Curr. Opin. Electrochem. 25 (2020) 100627. doi:10.1016/j.coelec.2020.08.009.

[15] C. Lo Vecchio, D. Sebastián, M.J. Lázaro, A.S. Aricò, V. Baglio, Non platinum-based cathode catalyst systems for direct methanol fuel cells, in: Direct Methanol Fuel Cell Technol., Elsevier Inc., 2020: pp. 289–316. doi:https://doi.org/10.1016/B978-0-12-819158-3.00010-0.

[16] D. Sebastián, A. Serov, I. Matanovic, K. Artyushkova, P. Atanassov, A.S. Aricò, V. Baglio, Insights on the extraordinary tolerance to alcohols of Fe-N-C cathode catalysts in highly performing direct alcohol fuel cells, Nano Energy. 34 (2017) 195–204. doi:10.1016/j.nanoen.2017.02.039.

[17] A.H.A. Monteverde Videla, D. Sebastián, N.S. Vasile, L. Osmieri, A.S. Aricò, V. Baglio, S. Specchia, Performance analysis of Fe-N-C catalyst for DMFC cathodes: Effect of water saturation in the cathodic catalyst layer, Int. J. Hydrogen Energy. 41 (2016) 22605–22618. doi:10.1016/j.ijhydene.2016.06.060.

[18] D. Banham, S. Ye, K. Pei, J.I. Ozaki, T. Kishimoto, Y. Imashiro, A review of the stability and durability of non-precious metal catalysts for the oxygen reduction reaction in proton exchange membrane fuel cells, J. Power Sources. 285 (2015) 334–348. doi:10.1016/j.jpowsour.2015.03.047.

[19] U. Martinez, S. Komini Babu, E.F. Holby, P. Zelenay, Durability challenges and perspective in the development of PGM-free electrocatalysts for the oxygen reduction reaction, Curr. Opin. Electrochem. 9 (2018) 224–232. doi:10.1016/j.coelec.2018.04.010.

[20] Y. Shao, J.P. Dodelet, G. Wu, P. Zelenay, PGM-Free Cathode Catalysts for PEM Fuel Cells: A Mini-Review on Stability Challenges, Adv. Mater. 31 (2019) 1–8. doi:10.1002/adma.201807615.

[21] J. Chen, X. Yan, C. Fu, Y. Feng, C. Lin, X. Li, S. Shen, C. Ke, J. Zhang, Insight into the Rapid Degradation Behavior of Nonprecious Metal Fe-N-C Electrocatalyst-Based Proton Exchange Membrane Fuel Cells, ACS Appl. Mater. Interfaces. 11 (2019) 37779–37786. doi:10.1021/acsami.9b13474.

[22]   L. Osmieri, Transition Metal–Nitrogen–Carbon (M–N–C) Catalysts for Oxygen Reduction Reaction. Insights on Synthesis and Performance in Polymer Electrolyte Fuel Cells, ChemEngineering. 3 (2019) 16. doi:10.3390/chemengineering3010016.

[23]   S. Kabir, S. Medina, G. Wang, G. Bender, S. Pylypenko, K.C. Neyerlin, Improving the bulk gas transport of Fe-N-C platinum group metal-free nanofiber electrodes via electrospinning for fuel cell applications, Nano Energy. 73 (2020) 104791. doi:10.1016/j.nanoen.2020.104791.

*[24] L. Jiao, J. Li, L.L. Richard, Q. Sun, T. Stracensky, E. Liu, Z. Zhao, F. Yang, S. Zhong, H. Xu, S. Mukerjee, Y. Huang, D.A. Cullen, D.J. Myers, F. Jaouen, Q. Jia, Chemical Vapor Deposition of Fe-N-C Oxygen Reduction Catalysts with Full Utilization of Dense Fe-N_4 Sites Chemical vapor deposition of Fe-N-C oxygen reduction catalysts with full utilization of dense Fe-N_4 sites, ChemRxiv. (2020). doi:10.26434/chemrxiv.12918983.v1.

An interesting paper showing how using chemical vapor deposition as synthesis method the activity of Fe-N-C can be tuned to improve the performace toward ORR thanks to an increase number of Fe-N_4 active sites fully used for the reaction.

[25]   R.K. Ahluwalia, X. Wang, L. Osmieri, J.-K. Peng, H.T. Chung, K.C. Neyerlin, Performance of Polymer Electrolyte Fuel Cell Electrodes with Atomically Dispersed (AD) Fe-C-N ORR Catalyst, J. Electrochem. Soc. 166 (2019) F1096–F1104. doi:10.1149/2.0851914jes.

[26]   P. Zelenay, D.J. Myers, ElectroCat (Electrocatalysis Consortium), 2020. https://www.hydrogen.energy.gov/pdfs/review20/fc160_myers_zelenay_2020_o.pdf.

[27]   U.I. Kramm, M. Lefèvre, N. Larouche, D. Schmeisser, J.P. Dodelet, Correlations between mass activity and physicochemical properties of Fe/N/C catalysts for the ORR in PEM fuel cell via 57Fe Mössbauer spectroscopy and other techniques, J. Am. Chem. Soc. 136 (2014) 978–985. doi:10.1021/ja410076f.

**[28] J.H. Zagal, M.T.M. Koper, Reactivity Descriptors for the Activity of Molecular MN4 Catalysts for the Oxygen Reduction Reaction, Angew. Chemie - Int. Ed. 55 (2016) 14510–14521. doi:10.1002/anie.201604311.

An outstanding review paper providing a view on reactivity descriptors of highly active PGM-free

catalysts.

[29] J. Li, F. Jaouen, Structure and activity of metal-centered coordination sites in pyrolyzed metal–nitrogen–carbon catalysts for the electrochemical reduction of O_2, Curr. Opin. Electrochem. 9 (2018) 198–206. doi:10.1016/j.coelec.2018.03.039.

[30] I. Martinaiou, A.H.A. Monteverde Videla, N. Weidler, M. Kübler, W.D.Z. Wallace, S. Paul, S. Wagner, A. Shahraei, R.W. Stark, S. Specchia, U.I. Kramm, Activity and degradation study of an Fe-N-C catalyst for ORR in Direct Methanol Fuel Cell (DMFC), Appl. Catal. B Environ. 262 (2020) 118217. doi:10.1016/j.apcatb.2019.118217.

[31] A.M. Patel, S. Ringe, S. Siahrostami, M. Bajdich, J.K. Nørskov, A.R. Kulkarni, Theoretical Approaches to Describing the Oxygen Reduction Reaction Activity of Single-Atom Catalysts, J. Phys. Chem. C. 122 (2018) 29307–29318. doi:10.1021/acs.jpcc.8b09430.

[32] A. Kulkarni, S. Siahrostami, A. Patel, J.K. Nørskov, Understanding Catalytic Activity Trends in the Oxygen Reduction Reaction, Chem. Rev. 118 (2018) 2302–2312. doi:10.1021/acs.chemrev.7b00488.

*[33] C.H. Choi, H.-K. Lim, M.W. Chung, G. Chon, N.R. Sahraie, A. Altin, M.-T. Sougrati, L. Stievano, H.S. Oh, E.S. Park, L. Fan, P. Strasser, G. Dražić, K.J.J. Mayrhofer, H. Kim, F. Jaouen, The Achilles' heel of iron-based catalysts during oxygen reduction in an acidic medium, Energy Environ. Sci. 11 (2018) 3176–3182. doi:doi.org/10.1039/C8EE01855C.

An interesting paper onrevealing deactivation mechanism of Fe-N-C- catalysts during ORR in acidic medium. FeN_xC_y moieties are structurally stable but electrochemically unstable when exposed in acidic medium to H_2O_2, which leaves iron-based catalytic sites untouched but decreases their turn-over frequency via oxidation of the carbon surface, leading to weakened O_2 binding on iron-based sites. The turn-over frequency is recovered upon electrochemical reduction of the carbon surface.

[34] J. Duch, P. Stelmachowski, A.H.A. Monteverde Videla, M. Gajewska, A. Kotarba, S. Specchia, Thermal oxygen activation followed by in situ work function measurements over carbon-supported noble metal-based catalysts, Int. J. Hydrogen Energy. 44 (2019) 16648–16656. doi:10.1016/j.ijhydene.2019.04.130.

[35] K. Yokoyama, Y. Sato, M. Yamamoto, T. Nishida, K. Motomiya, K. Tohji, Y. Sato, Work function, carrier type, and conductivity of nitrogen-doped single-walled carbon nanotube catalysts prepared by annealing via defluorination for efficient oxygen reduction reaction, Carbon N. Y. 142 (2019) 518–527. doi:10.1016/j.carbon.2018.10.052.

[36] J.H. Zagal, Electrochemistry, past, present, and future: energy conversion, sensors, and beyond, J. Solid State Electrochem. 24 (2020) 2195–2197. doi:10.1007/s10008-020-04707-x.

[37] M. Viera, J. Riquelme, C. Aliaga, J.F. Marco, W. Orellana, J.H. Zagal, F. Tasca, Oxygen Reduction Reaction at Penta-Coordinated Co Phthalocyanines, Front. Chem. 8 (2020) 1–12. doi:10.3389/fchem.2020.00022.

[38] J.H. Zagal, S. Specchia, P. Atanassov, Mapping Transition Metal-MN4 Macrocyclic Complex Catalysts Performance for the Critical Reactivity Descriptors, Curr. Opin. Electrochem. in press (2021). COELEC_100683.

[39] H.A. Gasteiger, S.S. Kocha, B. Sompalli, F.T. Wagner, Activity benchmarks and requirements for Pt, Pt-alloy, and non-Pt oxygen reduction catalysts for PEMFCs, Appl. Catal. B Environ. 56 (2005) 9–35. doi:10.1016/j.apcatb.2004.06.021.

**[40] M. Primbs, Y. Sun, A. Roy, D. Malko, A. Mehmood, M.-T. Sougrati, P.-Y. Blanchard, G. Granozzi, T. Kosmala, G. Daniel, P. Atanassov, J. Sharman, C. Durante, A. Kucernak, D.J. Jones, F. Jaouen, P. Strasser, Establishing Reactivity Descriptors for Platinum Group Metal (PGM)-free Fe-N-C Catalysts for PEM Fuel Cells, Energy Environ. Sci. (2020). doi:10.1039/d0ee01013h.

An outstanding paper reporting a comprehensive analysis of the oxygen reduction activity of four well-known Fe-N-C- catalysts from different laboratories. Maps of site density versus turn-over frequency are proposed as a rational tool for the engineering development of PGM-free catalysts.

[41] D. Malko, T. Lopes, E. Symianakis, A.R. Kucernak, The intriguing poison tolerance of non-precious metal oxygen reduction reaction (ORR) catalysts, J. Mater. Chem. A. 4 (2016) 142–152. doi:10.1039/c5ta05794a.

[42] A. Serov, K. Artyushkova, P. Atanassov, Fe-N-C oxygen reduction fuel cell catalyst derived from carbendazim: Synthesis, structure, and reactivity, Adv. Energy Mater. 4

(2014) 1–7. doi:10.1002/aenm.201301735.

[43]   Precious-Metal-Free (PMF) Catalysts, (n.d.). https://pajaritopowder.com/pmf-catalysts/ (accessed July 17, 2020).

[44]   K. Kumar, L. Dubau, M. Mermoux, J. Li, A. Zitolo, J. Nelayah, F. Jaouen, F. Maillard, On the Influence of Oxygen on the Degradation of Fe-N-C Catalysts, Angew. Chemie. 132 (2020) 3261–3269. doi:10.1002/ange.201912451.

*[45] J. Weiss, H. Zhang, P. Zelenay, Recent progress in the durability of Fe-N-C oxygen reduction electrocatalysts for polymer electrolyte fuel cells, J. Electroanal. Chem. 875 (2020) 114696. doi:10.1016/j.jelechem.2020.114696.

An interesting mini-review discussing the most prominent degradation mechanisms of Fe-N-C active site, that are demetallation and carbon corrosion, with emphasis on the role of H_2O_2 radicals. The paper also illustrates the recent advancements in the stability and durability of Fe-N-C- catalysts under PEMFC opration.

**[46]L. Osmieri, G. Wang, F.C. Cetinbas, S. Khandavalli, J. Park, S. Medina, S.A. Mauger, M. Ulsh, S. Pylypenko, D.J. Myers, K.C. Neyerlin, Utilizing ink composition to tune bulk-electrode gas transport, performance, and operational robustness for a Fe–N–C catalyst in polymer electrolyte fuel cell, Nano Energy. 75 (2020) 104943. doi:10.1016/j.nanoen.2020.104943.

An outstanding paper demonstrating how electrode optimization and electrode design can improve proton conductivity and bulk-electrode gas transport properties. These activities are critical for the improvement of PGM-free electrodes performance as much as the increases in catalyst activity and stability.

**[47]T. Marshall-Roth, N.J. Libretto, A.T. Wrobel, K. Anderton, N.D. Ricke, T. Van Voorhis, J.T. Miller, Y. Surendranath, A Pyridinic Fe-N4 Macrocycle Effectively Models the Active Sites in Fe/N-Doped Carbon Electrocatalysts, Chem. Rxiv. (n.d.) 1–21. doi:10.26434/CHEMRXIV.10008545.V1.

An outstanding paper elucidating that iron active sites in this class of materials exist in an Fe-N4 pyridinic ligation environment. Electrochemical data indicate that the iron center in (phen2N2)Fe displays excellent selectivity for 4-electron ORR This study provides a rich platform for constructing high-performance Fe-based oxygen reduction catalysts.

[48]   F. Luo, C.H. Choi, M.J.M. Primbs, W. Ju, S. Li, N.D. Leonard, A. Thomas, F.

Jaouen, P. Strasser, Accurate Evaluation of Active-Site Density (SD) and Turnover Frequency (TOF) of PGM-Free Metal-Nitrogen-Doped Carbon (MNC) Electrocatalysts using CO Cryo Adsorption, ACS Catal. 9 (2019) 4841–4852. doi:10.1021/acscatal.9b00588.

*[49] F. Luo, A. Roy, L. Silvioli, D.A. Cullen, A. Zitolo, M.T. Sougrati, I.C. Oguz, T. Mineva, D. Teschner, S. Wagner, J. Wen, F. Dionigi, U.I. Kramm, J. Rossmeisl, F. Jaouen, P. Strasser, P-block single-metal-site tin/nitrogen-doped carbon fuel cell cathode catalyst for oxygen reduction reaction, Nat. Mater. (2020). doi:10.1038/s41563-020-0717-5.

An interesting paper reporting the characterization of a Sn-N-C catalyst with high performance, with high selectivity tooward the 4-electron reduxction pathway. Here, stannic Sn(iv)Nx single-metal sites with moderate oxygen chemisorption properties and low pyridinic N coordination numbers act as catalytically active moieties.

[50] A. Zitolo, N. Ranjbar-Sahraie, T. Mineva, J. Li, Q. Jia, S. Stamatin, G.F. Harrington, S.M. Lyth, P. Krtil, S. Mukerjee, E. Fonda, F. Jaouen, Identification of catalytic sites in cobalt-nitrogen-carbon materials for the oxygen reduction reaction, Nat. Commun. 8 (2017) 1–10. doi:10.1038/s41467-017-01100-7.

*[51] D. Malko, A. Kucernak, T. Lopes, Performance of Fe–N/C Oxygen Reduction Electrocatalysts toward NO_2^-, NO, and NH_2OH Electroreduction: From Fundamental Insights into the Active Center to a New Method for Environmental Nitrite Destruction, J. Am. Chem. Soc. 138 (2016) 16056–16068. doi:10.1021/jacs.6b09622.

An interesting paper explaining in detail the procedure for the determination of the site density and turn-over frequency using the reversible nitrite adsorption followed by reductive stripping.

*[52] N.R. Sahraie, U.I. Kramm, J. Steinberg, Y. Zhang, A. Thomas, T. Reier, J.P. Paraknowitsch, P. Strasser, Quantifying the density and utilization of active sites in non-precious metal oxygen electroreduction catalysts, Nat. Commun. 6 (2015) 1–9. doi:10.1038/ncomms9618.

An interesting paper explaining in detail the effect of two or three heat treatments, in combination with one or two acid leaching, on monometallic Fe- and Mn-based and bimetallic FeMn-based catalysts, can increase the site density and turn-over frequency of the catalysts synthetized.

[53] F. Jaouen, M. Lefèvre, J.-P. Dodelet, M. Cai, Heat-treated Fe/N/C catalysts for O_2 electroreduction: Are active sites hosted in micropores?, J. Phys Chem B. 110 (2006) 5553–5558.

[54] T. Reshetenko, A. Serov, M. Odgaard, G. Randolf, L. Osmieri, A. Kulikovsky, Electron and proton conductivity of Fe-N-C cathodes for PEM fuel cells: A model-based electrochemical impedance spectroscopy measurement, Electrochem. Commun. 118 (2020) 106795. doi:10.1016/j.elecom.2020.106795.

[55] L. Osmieri, S. Mauger, M. Ulsh, K.C. Neyerlin, G. Bender, Use of a segmented cell for the combinatorial development of platinum group metal-free electrodes for polymer electrolyte fuel cells, J. Power Sources. 452 (2020). doi:10.1016/j.jpowsour.2020.227829.

[56] H.T. Chung, D.A. Cullen, D. Higgins, B.T. Sneed, E.F. Holby, K.L. More, P. Zelenay, Direct atomic-level insight into the active sites of a high-performance PGM-free ORR catalyst, Science (80-.). 357 (2017) 479–484. doi:10.1126/science.aan2255.

[57] L. Jiao, J. Li, L.L. Richard, T. Stracensky, E. Liu, Q. Sun, M.-T. Sougrati, Z. Zhao, F. Yang, S. Zhong, H. Xu, S. Mukerjee, Y. Huang, D.J. Myers, F. Jaouen, Q. Jia, High-Performance Iron-Based ORR Catalysts Synthesized via Chemical Vapor Deposition, ChemRxiv. (2019) 1–19. doi:10.26434/chemrxiv.10072475.v1.

[58] A. Zitolo, V. Goellner, V. Armel, M.T. Sougrati, T. Mineva, L. Stievano, E. Fonda, F. Jaouen, Identification of catalytic sites for oxygen reduction in iron- and nitrogen-doped graphene materials, Nat. Mater. 14 (2015) 937–942. doi:10.1038/nmat4367.

*[59] X. Wan, X. Liu, Y. Li, R. Yu, L. Zheng, W. Yan, H. Wang, M. Xu, J. Shui, Fe–N–C electrocatalyst with dense active sites and efficient mass transport for high performance proton exchange membrane fuel cells, Nat. Catal. 2 (2019) 259–268. doi:10.1038/s41929-019-0237-3.

An interesting paper explaining in detail how it is possible to obtain Fe-N-C catalysts dense of active sites by enhancing the external surface area and mesoporosity, to favor $Fe-N_4$ moieties exposed to oxygen.

[60] A.H.A. Monteverde Videla, L. Osmieri, M. Armandi, S. Specchia, Varying the

morphology of Fe-N-C electrocatalysts by templating Iron Phthalocyanine precursor with different porous SiO_2 to promote the Oxygen Reduction Reaction, Electrochim. Acta. 177 (2015) 43–50. doi:10.1016/j.electacta.2015.01.165.

[61]   J. Herranz, F. Jaouen, M. Lefèvre, U.I. Kramm, E. Proietti, J.P. Dodelet, P. Bogdanoff, S. Fiechter, I. Abs-Wurmbach, P. Bertrand, T.M. Arruda, S. Mukerjee, Unveiling N-protonation and anion-binding effects on Fe/N/C catalysts for O_2 reduction in proton-exchange-membrane fuel cells, J. Phys. Chem. C. 115 (2011) 16087–16097. doi:10.1021/jp2042526.

[62]   N. Ramaswamy, U. Tylus, Q. Jia, S. Mukerjee, Activity Descriptor Identification for Oxygen Reduction on Nonprecious Electrocatalysts: Linking Surface Science to Coordination Chemistry, J. Am. Chem. Soc. 135 (2013) 15443–15449. doi:10.1021/ja405149m.

**[63]J. Li, M.T. Sougrati, A. Zitolo, J.M. Ablett, I.C. Oğuz, T. Mineva, I. Matanovic, P. Atanassov, Y. Huang, I. Zenyuk, A. Di Cicco, K. Kumar, L. Dubau, F. Maillard, G. Dražić, F. Jaouen, Identification of durable and non-durable FeNx sites in Fe–N–C materials for proton exchange membrane fuel cells, Nat. Catal. (2020). doi:10.1038/s41929-020-00545-2.

An outstanding paper identifying durable and non-durable FeNx active sites on Fe–N–C catalysts for ORR. Fe–N–C catalysts initially comprising two distinct FeN$_x$ sites (S1 and S2, both contributing to the ORR activity), degrade via the transformation of S1 into iron oxides, while the structure and number of S2 were unmodified, remaining substantially the only active sites contributing to ORR after 50 h of operation in PEMFC.

**[64]X. Xie, C. He, B. Li, Y. He, D.A. Cullen, E.C. Wegener, A.J. Kropf, U. Martinez, Y. Cheng, M.H. Engelhard, M.E. Bowden, M. Song, T. Lemmon, X.S. Li, Z. Nie, J. Liu, D.J. Myers, P. Zelenay, G. Wang, G. Wu, V. Ramani, Y. Shao, Performance enhancement and degradation mechanism identification of a single-atom Co–N–C catalyst for proton exchange membrane fuel cells, Nat. Catal. 3 (2020). doi:10.1038/s41929-020-00546-1.

An outstanding paper explaining in detail two main degradation mechanisms for metal (M)–N–C catalysts: catalyst oxidation by radicals and active-site demetallation. An atomically dispersed Co–N–C catalyst showed comparable ORR catalytic activity to that of a similarly synthesized Fe–N–C catalyst,

but with a four-time enhanced durability. The enhanced durability of Co–N–C is attributed to the lower activity of Co ions for Fenton reactions and the significantly enhanced resistance to demetallation.

[65]   J.H. Zagal, M. Paez, J. Sturm, S. Ureta-Zanartu, Electroreduction of oxygen mixtures of phthalocyanines co-adsorbed on a graphite electrode, J. Electroanal. Chem. 181 (1984) 295–300.